Supplementary Information (SI) for Nanoscale.
This journal is © The Royal Society of Chemistry 2025

Supporting information:

Heat-treatment-induced enhancement of activity and stability in Rh/Mo-doped PtNi octahedra for the oxygen reduction reaction

P. Paciok[a], S. Polani[b], R. Amitrano[b], T. Möller[b], O. Prymak[c], J. Kang[b], M. Klingenhof[b], K. MacArthur[ad], H. Matsumoto[e], M. Heggen[a], P. Strasser[b] and R. E. Dunin-Borkowski[a]

a. *Ernst Ruska-Center for Microscopy and Spectroscopy with Electrons (ERC), Forschungszentrum Jülich GmbH, Jülich 52425, Germany.*
b. *Electrochemical Energy, Catalysis and Material Science Laboratory, Department of Chemistry, Technical University Berlin, 10623 Berlin, Germany.*
c. *Inorganic Chemistry and Center for Nanointegration Duisburg-Essen (CENIDE), University of Duisburg-Essen, Universitaetsstr. 7, 45141 Essen, Germany.*
d. *Oxford Instruments Materials Analysis, High Wycombe, Buckinghamshire, United Kingdom.*
e. *Core Technology & Solutions Business Group, Hitachi High-Tech Corporation, 882 Ichige, Hitachinaka, Ibaraki 312-8504, Japan*

Experimental Procedures

Materials.

Platinum (II) acetylacetonate (Pt(acac)2, ≥98%) was obtained from Acros, nickel (II) acetylacetonate (Ni(acac)2, ≥98%), rhodium acetylacetonate (Rh(acac)3, 97.0%), molybdenum hexacarbonyl (Mo(CO)6, 99.9%), and Nafion solution (5% w/w) were obtained from Sigma Aldrich. Polyvinylpyrrolidone (M. W. 10,000) and benzoic acid (99%) were obtained from Alfa Aesar. Benzyl alcohol (≥99%) was purchased from Carl-Roth, acetone (≥99%) and ethanol (absolute) were purchased from VWR International. Carbon black (Vulcan XC -72) was obtained from Cabot Corporation. All chemicals were used as received.

Synthesis of PtNi/C octahedral NPs.[1]

Synthesis of PtNi/C Ni-rich with 6 nm edge length, PtNi: 64 mg $Pt(acac)_2$, 200 mg $Ni(acac)_2$, 0.64 g PVP (10k) and 0.4 g benzoic acid in 40 mL benzyl alcohol (BA). The 100 mL pressure glass flask was then stoppered and stirred vigorously for 1 h at RT. Afterwards the flask was heated to 150 ℃ with a ramp of 5 ℃ min^{-1}. After 12 h of reaction, the reaction solution was allowed to cool to RT, and then 100 mg of carbon (XC 72R), which had been pre-dispersed in 10 mL of BA by ultrasonication, was added to the reaction solution. After stirring overnight, the solution was purified with a mixture of ethanol and acetone using a centrifuge.

Synthesis of PtNiRhMo/C octahedral NPs.

In a typical synthesis of PtNiRhMo/C Ni-rich with 9 nm edge length: 64 mg $Pt(acac)_2$, 200 mg $Ni(acac)_2$, 20 mg $Mo(CO)_6$, 20 mg $Rh(acac)_3$, 64 g PVP (10k) and 0.4 g benzoic acid in 40 mL BA. The 100 mL pressure glass flask was then stoppered and placed in a heating mantle for 1 h with vigorous stirring at 60 ℃. Then the flask was heated to 150 ℃ with a ramp of 5 ℃ min^{-1}. After 12 h of reaction, the reaction solution was allowed to cool to RT, and then 100 mg of carbon (XC 72R), which had been pre-dispersed in 10 mL of BA by ultrasonication, was added to the reaction solution. After stirring overnight, the solution was purified with a mixture of ethanol and acetone using a centrifuge.

Heat-treatment

The catalyst was finely ground and distributed as evenly as possible in a lidded ceramic crucible. The lid was used to minimize powder loss due to the gas flow, as the light catalyst particles could otherwise be displaced in the oven. The crucible was positioned centrally within the oven to ensure uniform heating. To purge the chamber of residual oxygen, nitrogen was introduced at the same flow rate intended later for H_2 (4% in an Ar atmosphere), and flushed through for 30 minutes. Subsequently, the gas atmosphere was switched to H_2 (4% in an Ar atmosphere) for another 30 minutes. The sample was then heated to 350 °C at a rate of 5 K/min and maintained at that temperature for 2 hours. Following the heat treatment, the catalyst was allowed to cool naturally to approximately 50–60 °C, after which the gas flow was switched back to nitrogen and maintained until the chamber had cooled to room temperature.

Morphological, Structural and Elemental Characterization.

High resolution (HR)TEM and scanning TEM-energy dispersive spectroscopy (STEM-EDS).

High-resolution high-angle annular dark-field (HAADF) imaging and EDS elemental mapping were performed using a probe-corrected FEI Titan G2 80–200 (ChemiSTEM) scanning transmission electron microscope equipped with a four-quadrant Super-X energy dispersive X-ray spectrometer (EDS) system with a nominal solid angle of 0.7 srad. The experiments were carried out at an accelerating voltage of 80 kV to minimize particle damage and maximize X-ray counts, using a probe convergence angle of 25 mrad. The microscope was operated at spot size 6 and gun lens 5, yielding a probe diameter of ~0.1 nm and a current of ~60 pA. Samples were dispersed in ethanol, drop-casted onto Cu TEM grids (Plano GmbH, S160), dried in ambient air at room temperature, and subsequently dried in a vacuum oven (2×10^{-2} mbar, 75 °C, 16 h). Data acquisition and quantification were carried out using Velox 2.16.0.12. EDX spectrum imaging was typically performed with (250–400) × (250–400) pixels, a dwell time of 14

µs per pixel and 600 accumulated frames, corresponding to acquisition times between ~9 and 22 min per map (on average ~15 min). The actual duration depended on the area of interest, since larger particles required larger pixel arrays. Most measurements were carried out at a magnification of ~640 k, which ensured that the particles were well resolved within the pixel array while maintaining particle stability under the beam. The chosen acquisition conditions represented a good compromise between spatial resolution and measurement time. To minimize beam-induced changes, care was taken not to exceed these conditions. Particles size evaluation were conducted with the software imageJ. For each evaluation at least 150 different particles were analysed.

STEM-EDX on Hitachi HF5000

High-resolution STEM-EDX measurements of (seed) particles were performed on a Hitachi HF5000 environmental STEM operated at 80 kV in HR mapping mode with a convergence semi-angle of ≈25 mrad. Spectrum images were typically acquired with frame sizes between (250–400) × (250–400) pixels, a dwell time of 14 µs per pixel and 600 frame accumulations. Depending on the selected area of interest and the particle size, the total acquisition time per map ranged from approximately 9 to 23 min, corresponding to an average of ~15 min per map. Most EDX measurements were carried out at a nominal magnification of ~600k, which ensured that the particles were sufficiently resolved within the pixel array while minimizing the electron dose. This setting provided a suitable compromise between spatial resolution and acquisition time. To minimize beam-induced changes, the acquisition conditions were not exceeded. Data evaluation was carried out using the Oxford Instruments AztecEnergy 4.4 software.

It should be noted that weak Ti signals originated from the double-tilt holder, while Cu peaks arose from the spring clip used to secure the grid in the holder.

Identical location (IL) -STEM measurements.

10 µL of an aqueous catalyst suspension was drop-cast onto a gold TEM finder grid (S147A9, Plano GmbH) and left to dry at room temperature in ambient air. Subsequently, the grid was dried in a vacuum oven (2×10^{-2} mbar, 75 °C) for 16 h. After insertion into a FEI double-tilt low-background TEM holder and transfer to the Titan G2 80–200, several high-angle annular dark-field STEM images and corresponding elemental maps of different regions in the centre of the grid were acquired. Subsequently, the catalyst-coated TEM grid was mounted as the working electrode in a custom-made three-electrode glass cell equipped with a Luggin capillary. The grid was fixed between two glassy carbon plates using a Teflon band, with approximately half of the grid protruding from the GC-plate sandwich such that the pre-characterised locations were just outside the plate edge and thus exposed to the electrolyte. For improved electrical contact, a folding mesh with locking flap (Plano GmbH, G231A) was placed over the part of the grid embedded in the GC-plate sandwich.

The distance between the Luggin capillary tip and the working electrode was approximately 1 cm. The working and counter electrode compartments were separated by a glass frit, and the graphite rod counter electrode was positioned ~4 cm from the working electrode. A Gaskatel HydroFlex RHE was used as the reference electrode, positioned at the Luggin capillary inlet. The potential was controlled with a Bio-Logic Science Instruments SP-50 potentiostat, and the ohmic potential drop (iR drop) was measured and corrected using the current interrupt method. The accelerated stress test (AST) consisted of 10800 cycles between 0.6 and 0.95 V_{RHE} at 1 V s^{-1} in Ar-saturated 0.1 M $HClO_4$ at room temperature.

Prior to each experiment, all cell components (glass cell, GC plates, and gas inlet frit) were cleaned in aqua regia, thoroughly rinsed three times with ultrapure water, and dried in a vacuum oven. After AST, the grid was rinsed with ultrapure water to remove electrolyte residues, dried again in vacuum (2×10^{-2} mbar, 75 °C), and subsequently analysed at the identical pre-characterised locations.

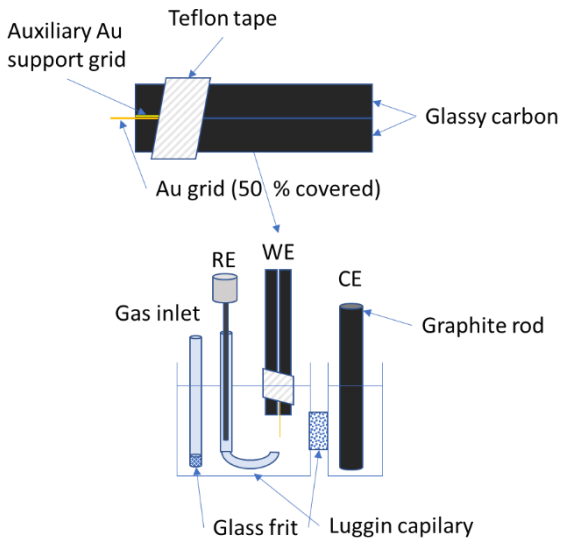

Figure S1 Schematic illustration of the identical location STEM electrochemical cell setup. The working electrode (WE) consisted of a catalyst-coated Au finder grid (S147A9, Plano GmbH) mounted between two glassy carbon plates using Teflon tape, with approximately 50 % of the grid protruding from the sandwich and exposed to the electrolyte. An auxiliary Au support grid (Plano GmbH, G231A) with locking flap was placed over the covered half of the grid to improve electrical contact. The counter electrode (CE) was a graphite rod positioned ~4 cm from the WE and separated by a glass frit. The reference electrode (RE; Gaskatel HydroFlex RHE) was positioned ~1 cm from the WE via a Luggin capillary. The cell was equipped with a gas inlet for Ar purging of the electrolyte.

X-ray photoelectron spectroscopy (XPS)

Measurements were performed using a PHI5000 VersaProbe II X-ray photoelectron spectrometer equipped with monochromatic Al Kα X-ray radiation. An accelerating voltage of 15 kV and a power of 50 W were used. All measurements, including sample preparation, were carried out at the ZEA-3 Institute of Analytics at Forschungszentrum Jülich. A silicon wafer covered with vacuum-stable, double-sided adhesive tape was used as a sample holder. A small amount of catalyst powder (approximately a spatula tip) was dispersed onto the adhesive tape before transferring the sample into the spectrometer. The X-ray spectra were analysed using the NIST XPS database and MULTIPAK software.

Inductively coupled plasma - optical emission spectrometry (ICP-OES)

ICP-OES was used to determine the elemental composition of the various catalysts. Samples were prepared by dissolving the catalyst powders in a mixture of H_2SO_4, HNO_3 and HCl (1:1:3). The solutions were heated from room temperature to 180 °C in 10 min using a Microwave Discover SP -D (CEM Corporation) and maintained at this temperature for 20 min. Finally, the solutions were diluted with Milli-Q® water, filtered and brought to a known volume. To calculate the concentration of the different solutions, 5 standards were prepared for Pt, Ni and Mo with concentrations of 0, 1, 4, 7 and 12 mg/L of each element.

In situ XRD

The in-situ X-ray diffraction (XRD) experiments were performed on a D8 advanced X-ray diffractometer equipped with a Goebel mirror, a position-sensitive LynxEye detector (PSD), and an external radiation heating chamber (MRI Physikalische Geräte GmbH, Tübingen,Germany). The heating chamber was positioned on the goniometer of the diffractometer, consisting of an AlCr foil as heater, an Al_2O_3 crucible as sample holder and a thermocouple. The Cu Ka tube was operated at a voltage of 40 kV and

a current of 40 mA. The Al_2O_3 crucible was filled with 20-30mg of catalyst powder (on carbon black support) and subsequently flattened to form a smooth surface. The temperature time protocol started with an initial XRD scan at 30°C and then heated up with 0.0167 °C s-1 to 350°C under 4% H2 in Ar with a flow rate of 40mLmin^{-1}. After a holding time of 30 min, XRD profiles were acquired. The XRD scanning parameters were: a 2V range from 32.5 to 55, a step size of 0.038, a holding time of 3 s per step, a fix divergence slit of 2 mm, a PSD iris anti-scattering slit of 13, and sample rotation. After careful instrumental parameter correction with the reference powder material Al_2O_3 (measured separately at room temperature), quantitative Rietveld refinement was performed with the software TOPAS 7.0 from Bruker to calculate the lattice parameters and the average crystallite size from diffraction peak broadening. At the same time, the detected reflection peaks of Al_2O_3 in the samples (nanoparticles) were also used for the precise determination of the sample displacement as refined in the Rietveld procedure.

In situ STEM

The in-situ experiments were performed on a Hitachi HF5000 environmental scanning transmission electron microscope operated at an accelerating voltage of 200 kV with a convergence semi-angle of ≈25 mrad. For the experiments, 2 µL of an aqueous catalyst dispersion was drop-casted onto a MEMS heating chip (NORCADA Inc., Canada), dried in ambient air for 2 h, and subsequently dried in a vacuum oven (2×10^{-2} mbar, 75 °C, 16 h). The chip was then transferred into the microscope using a Hitachi single-tilt heating holder. After insertion of the holder, the microscope was switched into in-situ mode, in which the two ion getter pumps (IGPs) located near the specimen area were isolated by closing the corresponding valves, and an additional turbomolecular pump (TMP) was engaged to maintain a low column pressure during gas introduction. To remove organic contaminants, the chip was first heated to 200 °C for 30 min in vacuum. An internal mass flow controller was then used to introduce H_2 at a flow rate of 3 sccm, corresponding to a pressure of ≈5 Pa near the sample. The temperature was subsequently increased to 300 °C at a rate of 3 °C s^{-1} under continuous H_2 flow.

Electrochemical Measurements.

A typical three-electrode cell was used to perform the electrochemical measurements. A rotating disk electrode (RDE) made of glassy carbon (0.196 cm², Pine Instrument) served as the working electrode. A hydrogen reference electrode (Gaskatel, HydroFlex) and a Pt mesh (5 × 5 cm²) rolled into a cylindrical shape and mounted on a Pt wire were used as reference and counter electrodes, respectively.

A catalyst ink was prepared by mixing 5.5 mg of the as-prepared catalyst powders (PtNi/C and PtNiRhMo/C) in water, isopropanol, and Nafion (v/v/v = 3.98 mL / 1.00 mL / 0.01 mL, total volume 4.99 mL) and sonicated for 45 min using an ultrasonic horn sonicator in an ice bath. 10 µL of the catalyst ink were dropped onto the working electrode and dried at 60 °C for 7 min. The loading amount of Pt for the octahedral PtNi and PtNiRhMo/C catalysts was 1.3–1.5 μg_{Pt}.

Cyclic voltammetry (CV) measurements were performed in N_2-saturated 0.1 M $HClO_4$. The electrodes were activated by 50 CV cycles at 100 mV s^{-1}, followed by CV cycles at 20 mV s^{-1} for electrochemical surface area (ECSA) determination. ECSAs were obtained from (i) the charge associated with hydrogen adsorption/desorption (H_{upd}, assuming 210 µC cm^{-2} for a full monolayer of H on Pt) and (ii) the CO-stripping charge (assuming 420 µC cm^{-2} for a full monolayer of CO on Pt). All electrochemical measurements (except for PtNi-F) were reproduced on two to three independently prepared RDE films to ensure consistency. For CO-stripping experiments, CO was adsorbed by holding the potential at 0.05 V vs. RHE in a CO-saturated 0.1 M $HClO_4$ solution for 25 min. Subsequently, the electrolyte was purged with N_2 for 35 min to remove dissolved CO. CO stripping was then performed by cycling the potential between 0.05 and 1.0 V vs. RHE at a scan rate of 50 mV s^{-1} in N_2-saturated electrolyte

For oxygen reduction reaction (ORR) measurements, the electrolyte was bubbled with O_2 for 20 min, after which the gas inlet was positioned just above the electrolyte surface to maintain an O_2 cushion during the measurements. Analogously, N_2 saturation was carried out for 20 min before background measurements, with the bubbler kept above the electrolyte during data acquisition. Linear sweep voltammetry (LSV) was performed at 20 mV s^{-1} with a rotation rate of 1600 rpm. To obtain the kinetic current densities (j_{kin}), the LSV curves measured in O_2-saturated solution were corrected by the

corresponding N_2 background currents. The diffusion-limited current density (J_{diff}) at 0.4 V vs. RHE was used to calculate J_{kin} at 0.9 V vs. RHE using the Koutecký–Levich relation:

1. $j_{kin} = (j^* j_{diff}) / (j_{diff} - j)$

where j is the measured current density, j_{diff} the diffusion-limited current density, and j_{kin} the kinetic current density.
Specific activity (SA) and mass activity (MA) were then derived from j_{kin} normalized to ECSA and Pt loading, respectively. The uncompensated resistance was determined by potentiostatic electrochemical impedance spectroscopy (PEIS), and all potentials were corrected for iR-drop.
Accelerated stress tests (ASTs) were performed by cycling the potential between 0.6 and 0.95 V vs. RHE at 1 V s^{-1} for 10 800 cycles in Ar-saturated 0.1 M $HClO_4$ at room temperature. These protocols follow established procedures used in recent work on PtNi-based catalysts.[1,3,4]
Tafel analysis was performed by plotting the electrode potential E_{RHE} against the decimal logarithm of the kinetic current density, Linear fits were applied in the kinetically controlled region, defined as $0.3 < |j|/|jL| < 0.5$, where j_L is the diffusion-limited current density

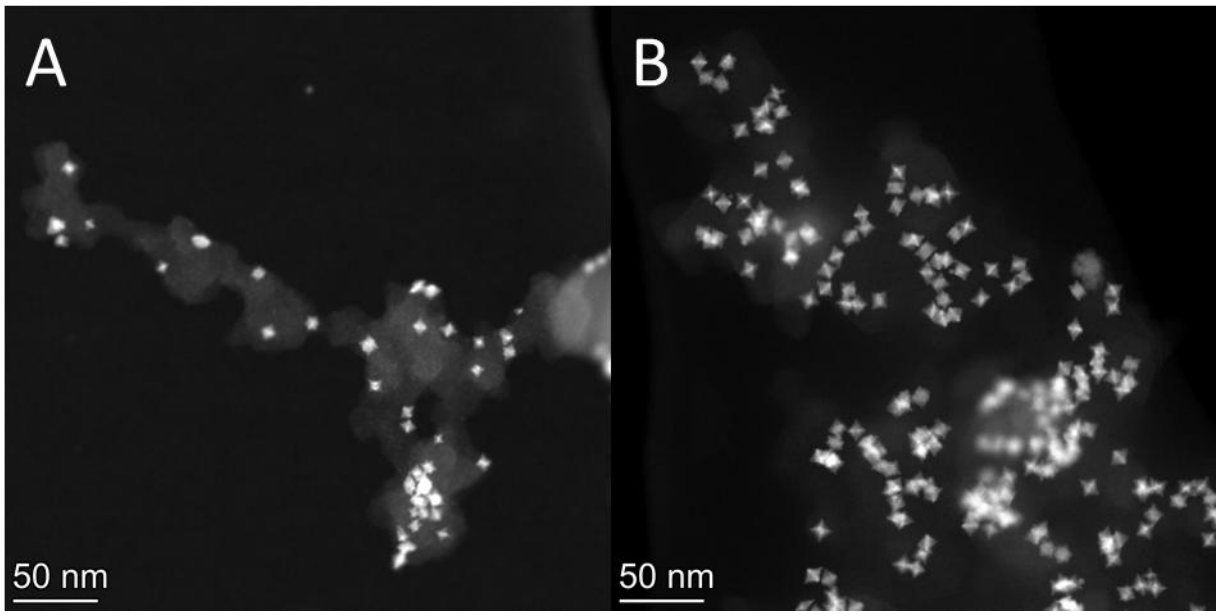

Figure S2 Overview HAADF images of the two samples A) PtNi-F and B) PtNiMoRh-F recorded with the FEI Titan G2 80 – 200 (at 80 kV) at a low magnification.

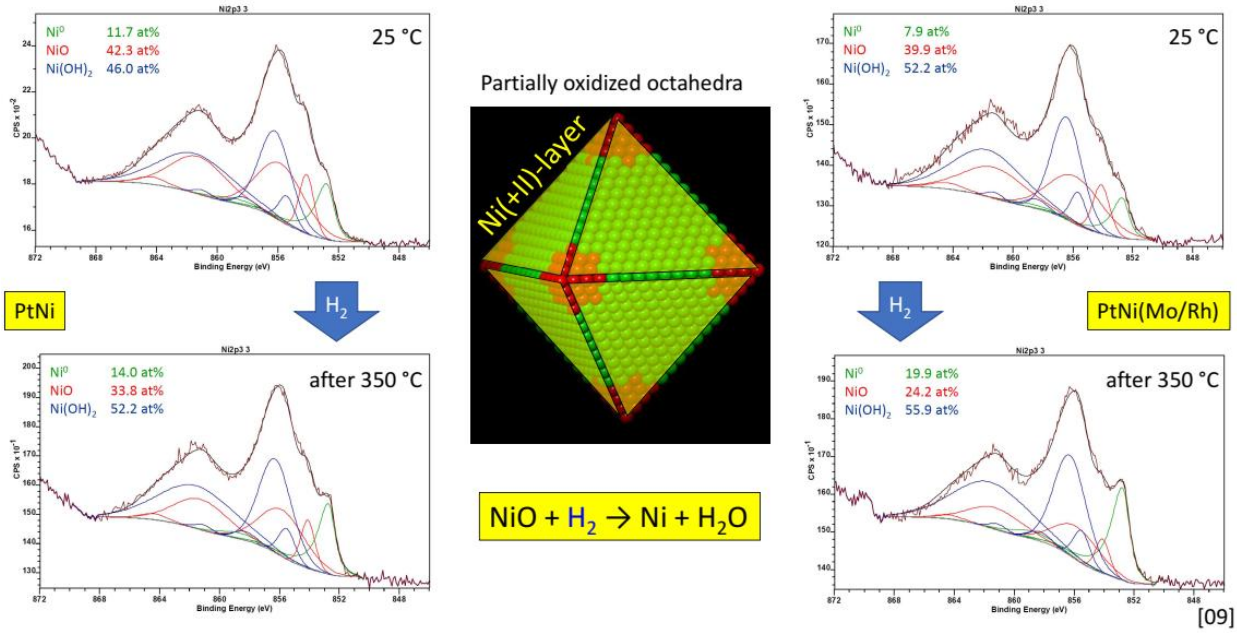

Figure S3 XPS spectra of PtNi (left) and PtNiMoRh (right) before and after a reductive heat treatment in H_2/Ar (4:96) at 350°C for 1 h..

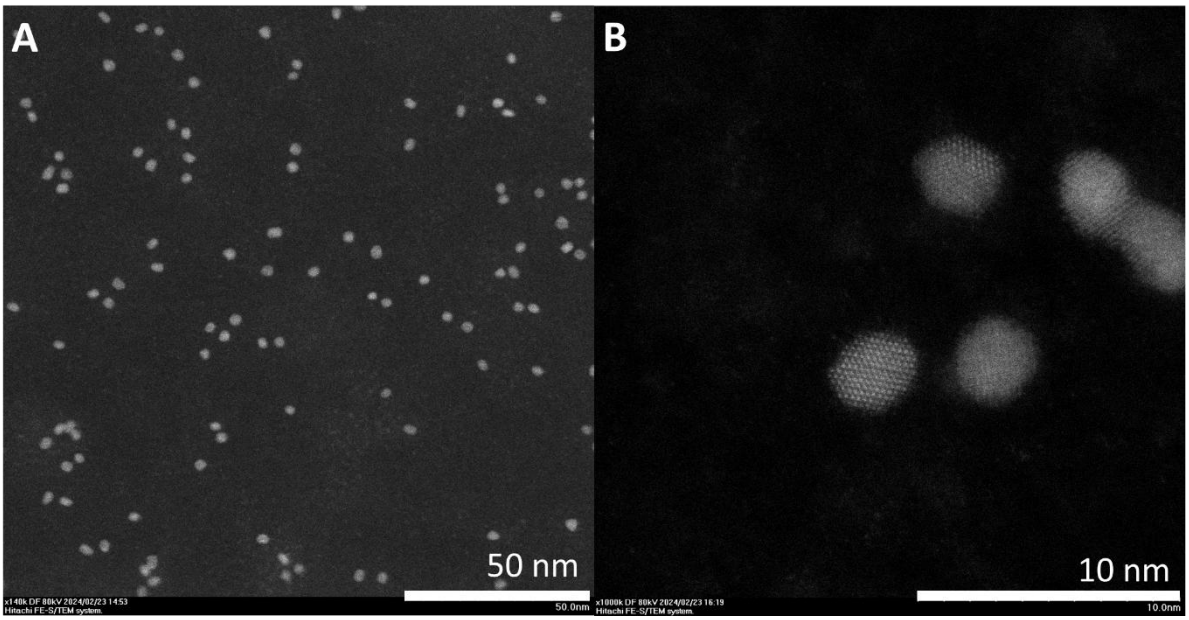

Figure S4 A) overview image of PtNiMoRh particles after 2 h reaction time; B) high resolution image of PtNiMoRh particles after 2 h reaction time recorded with a Hitachi HF5000 microscope at 80 kV.

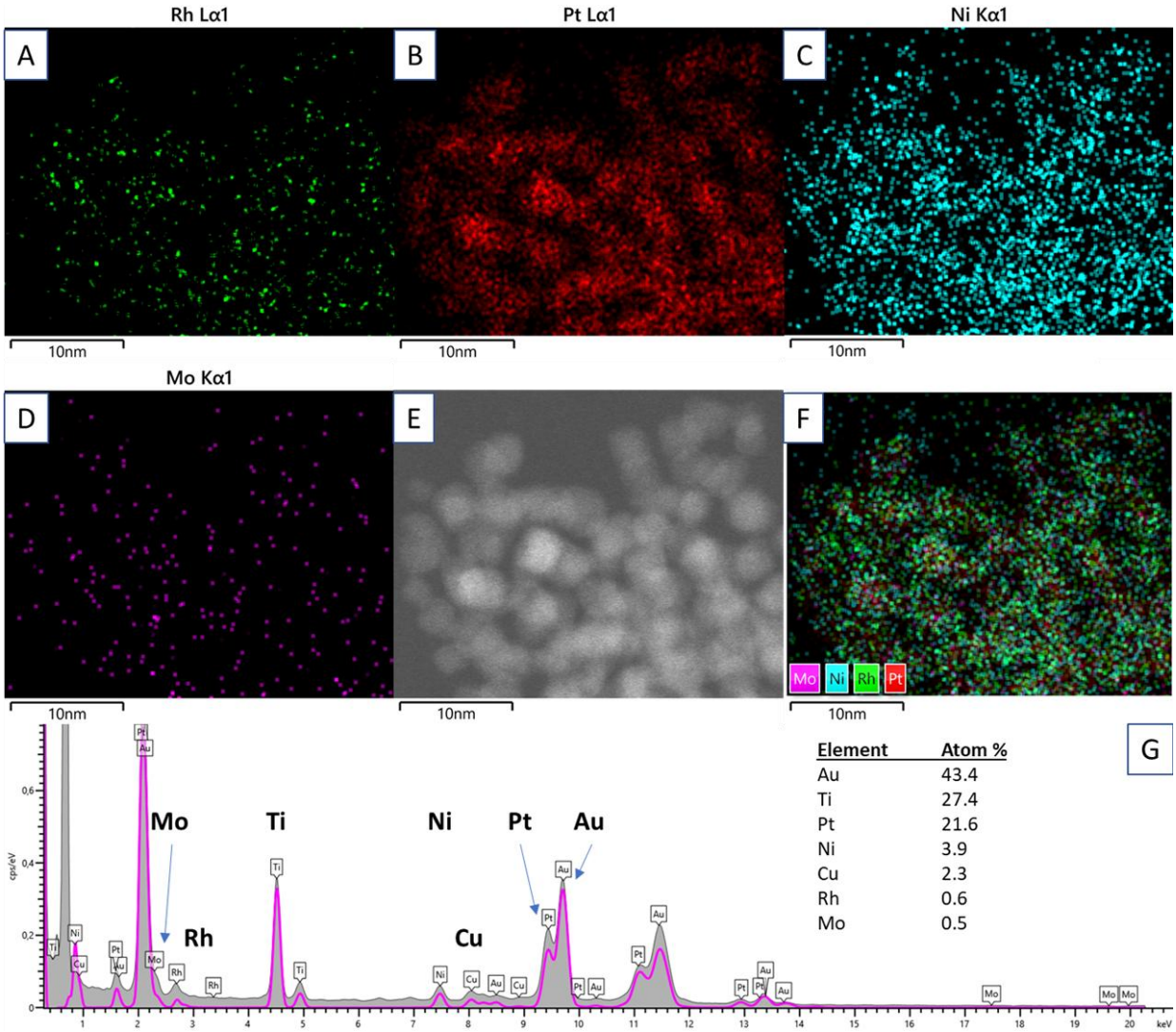

Figure S5 HAADF-STEM image, corresponding EDX elemental maps, and EDX spectrum of Pt-rich particles obtained after 2 h reaction time. (A) Rh Lα map (green), (B) Pt Lα map (red), (C) Ni Kα map (cyan), (D) Mo Kα map (magenta), (E) HAADF-STEM image, (F) overlay of Pt (red), Ni (cyan), Rh (green), and Mo (magenta) maps. (G) Corresponding EDX spectrum showing the full energy range with labelled peaks for Pt M (~2.05 keV), Mo Lα (~2.29 keV), Rh Lα (~2.70 keV), Ni Kα (7.47 keV), Pt Lα (9.44 keV), and Au M/L lines from the TEM support grid. Cu Kα/Kβ peaks (~8.04/8.90 keV) originate from the copper spring clip holding the grid in the TEM holder, and Ti Kα/Kβ peaks (~4.51/4.93 keV) stem from the double-tilt holder body. EDX data were acquired on a Hitachi HF5000 equipped with an AztecEnergy EDS system (Oxford Instruments) and two Ultim Max TLE detectors at 80 kV, using a pixel dwell time of 20 µs over 600 frames. Spectra were processed with Aztec 4.4 software, and peak deconvolution was applied. Due to the small particle size and partial peak overlap, Mo and Rh are reported as qualitative detections.

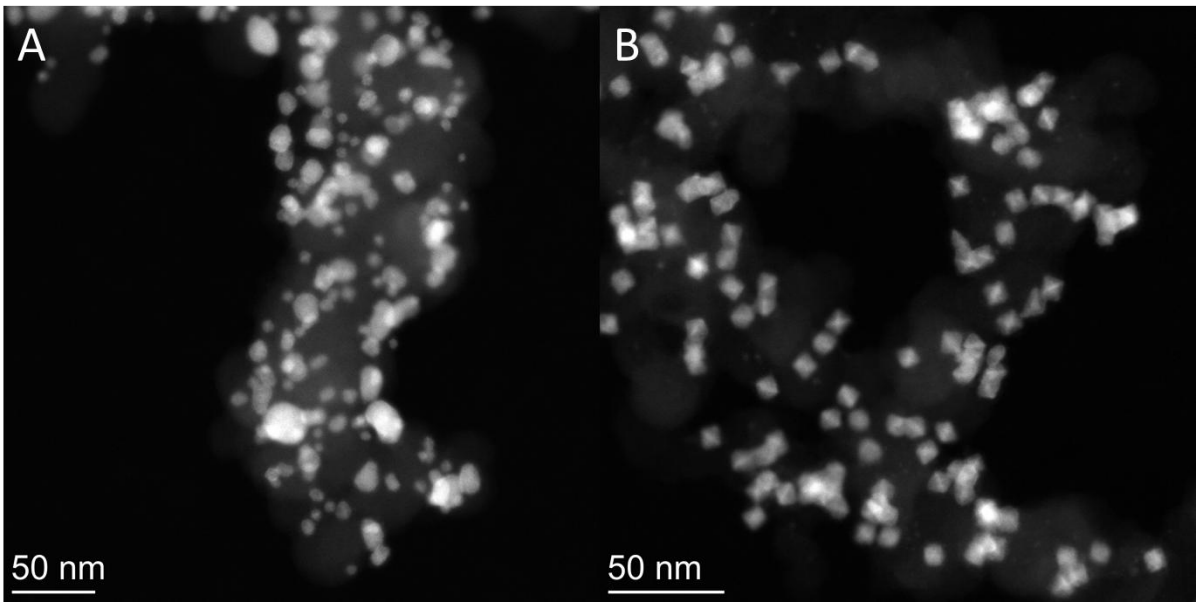

Figure S6 Ex-situ in H_2 (4%H_2 in Argon) at 350°C heat-treated A) PtNi-H and B) PtNiMoRh-H octahedra. The images were recorded with the Titan G2 80 -200 at an acceleration voltage of 80 kV.

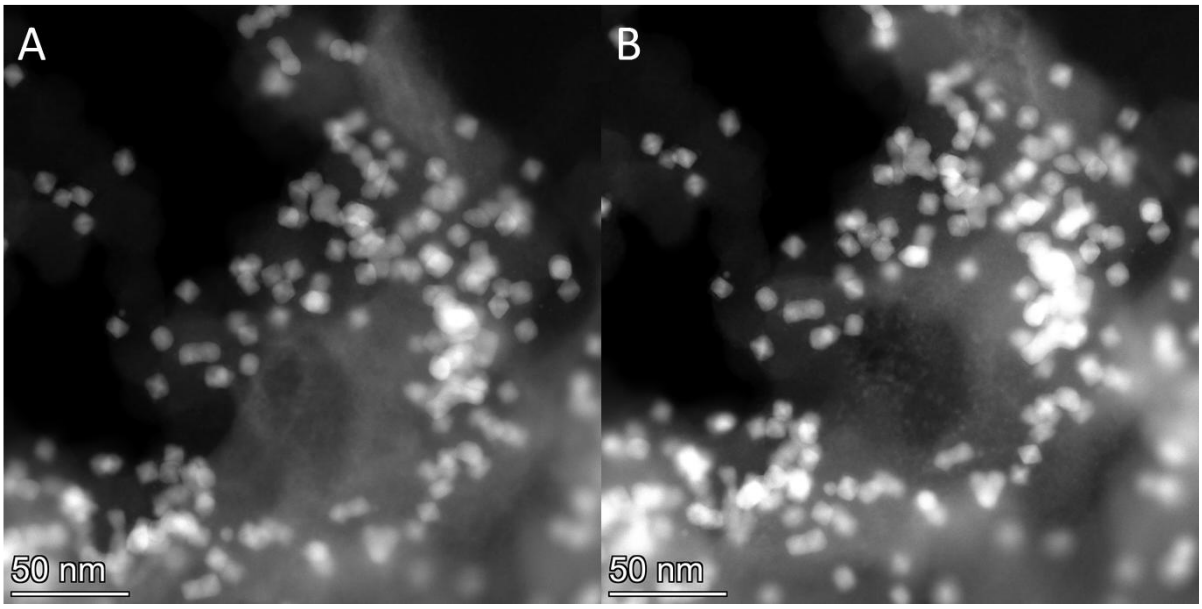

Figure S7 Overview HAADF images of PtNiMoRh-H particles A) before and B) after 10800 cycles between 0.6 and 0.95 V_{RHE} in Ar-saturated 0.1M $HClO_4$ at identical location. The images were recorded with the Titan G2 80 -200 at an acceleration voltage of 80 kV.

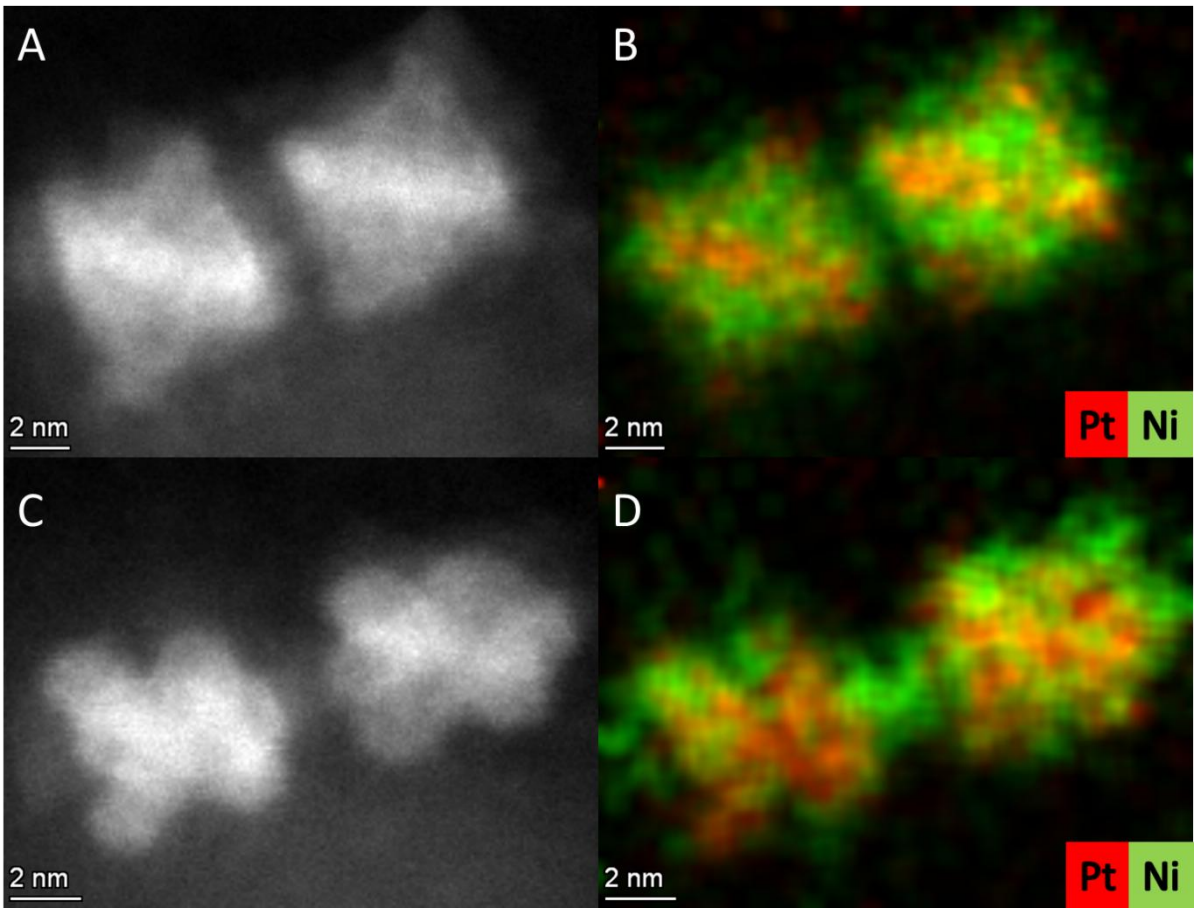

Figure S8 Representative HAADF images and EDX elemental maps of PtNi-F particles A,B) before and C,D) after) after 10800 cycles between 0.6 and 0.95 V_{RHE} in Ar-saturated 0.1M $HClO_4$ at identical location. The images were recorded with the Titan G2 80 -200 at an acceleration voltage of 80 kV.

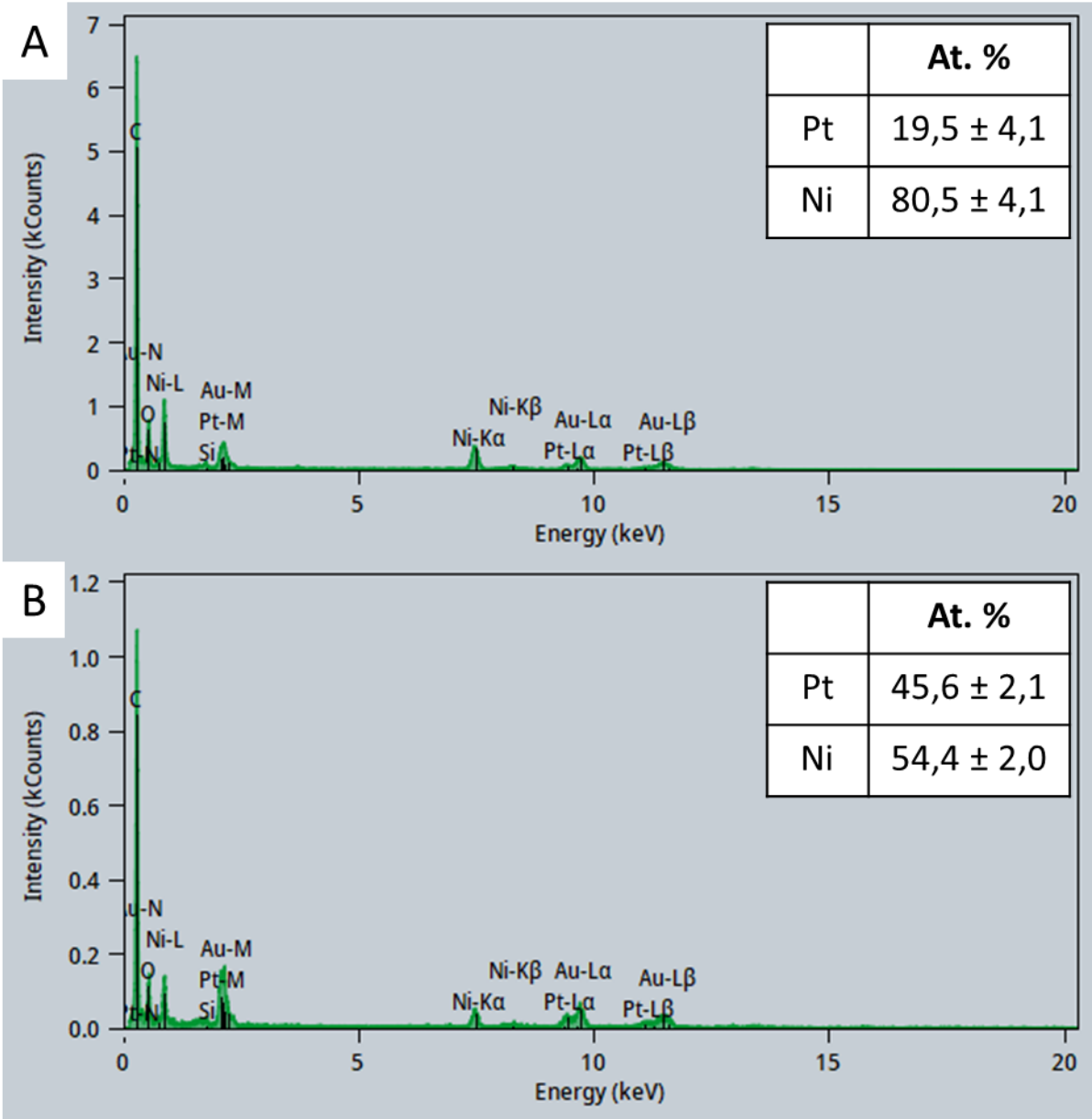

Figure S9 Representative EDX spectra of PtNi-F before (A) and after (B) an accelerated stress test (AST) consisting of 10800 potential cycles between 0.60 and 0.95 V_{RHE} in Ar-saturated 0.1 M $HClO_4$ at room temperature. Spectra were acquired on a FEI Titan G2 80–200 operated at 80 kV. For quantitative analysis of the Pt/Ni atomic ratio, 10 individual particles were examined before and after the AST at identical locations. The Au and Si peaks originate from the TEM support grid.

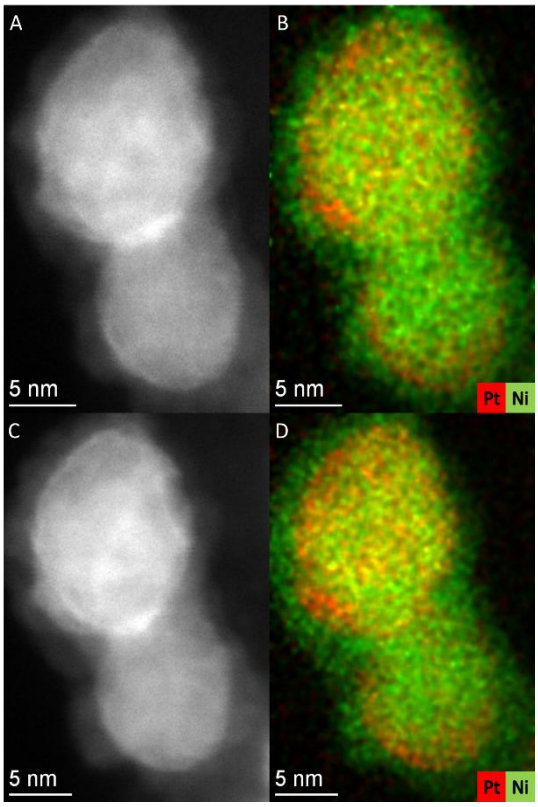

Figure S10 Representative HAADF images and EDX elemental maps of PtNi-H particles A, B) before and C,D) after 10800 cycles between 0.6 and 0.95 V_{RHE} in Ar-saturated 0.1M $HClO_4$ at identical location. The images were recorded with the Titan G2 80 -200 at an acceleration voltage of 80 kV.

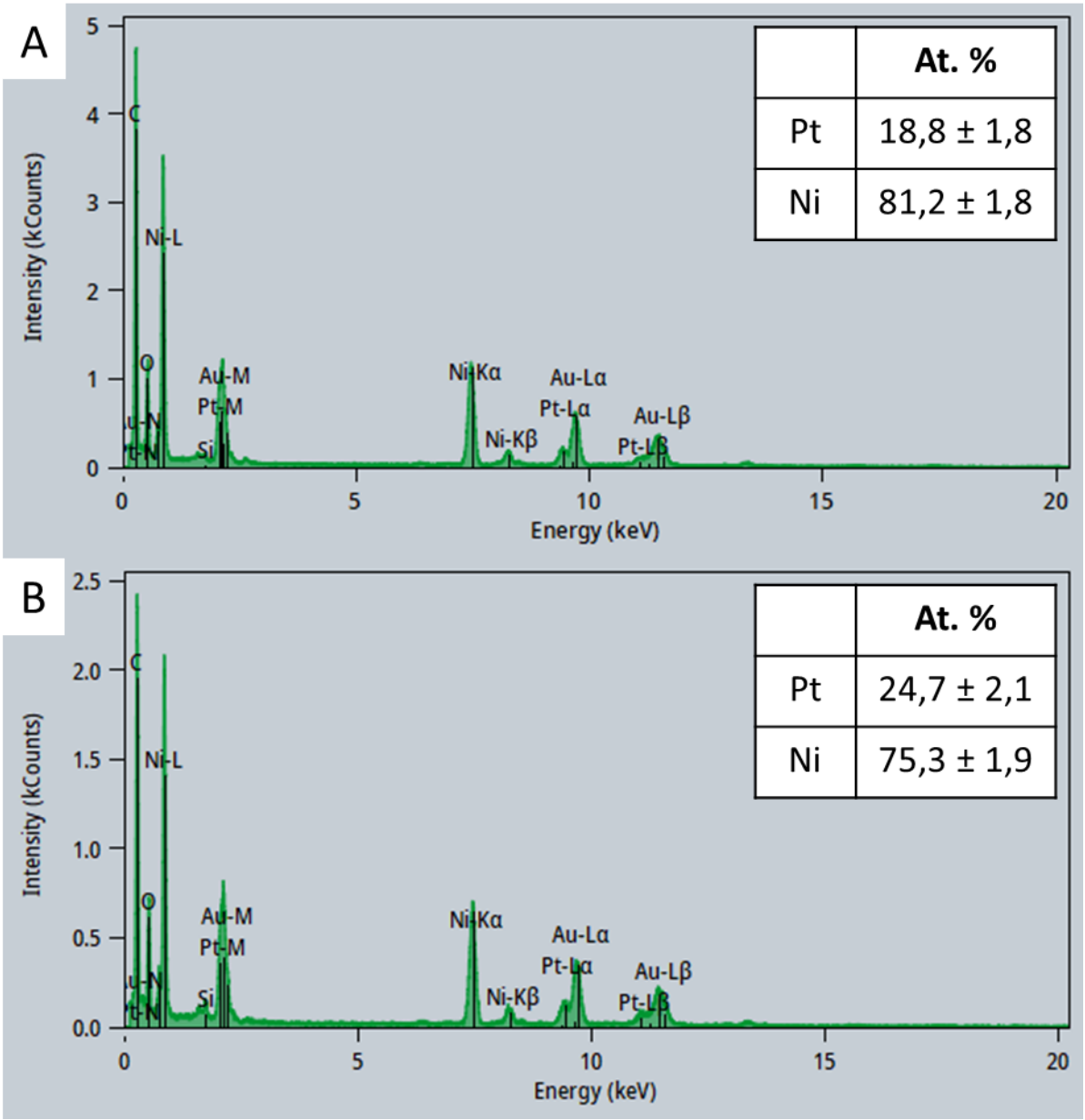

Figure S11 Representative EDX spectra of PtNi-H before (A) and after (B) an accelerated stress test (AST) consisting of 10 800 potential cycles between 0.60 and 0.95 V_{RHE} in Ar-saturated 0.1 M $HClO_4$ at room temperature. Spectra were acquired on a FEI Titan G2 80–200 operated at 80 kV. For quantitative analysis of the Pt/Ni atomic ratio, 10 individual particles were examined before and after the AST at identical locations. The Au and Si peaks originate from the TEM support grid.

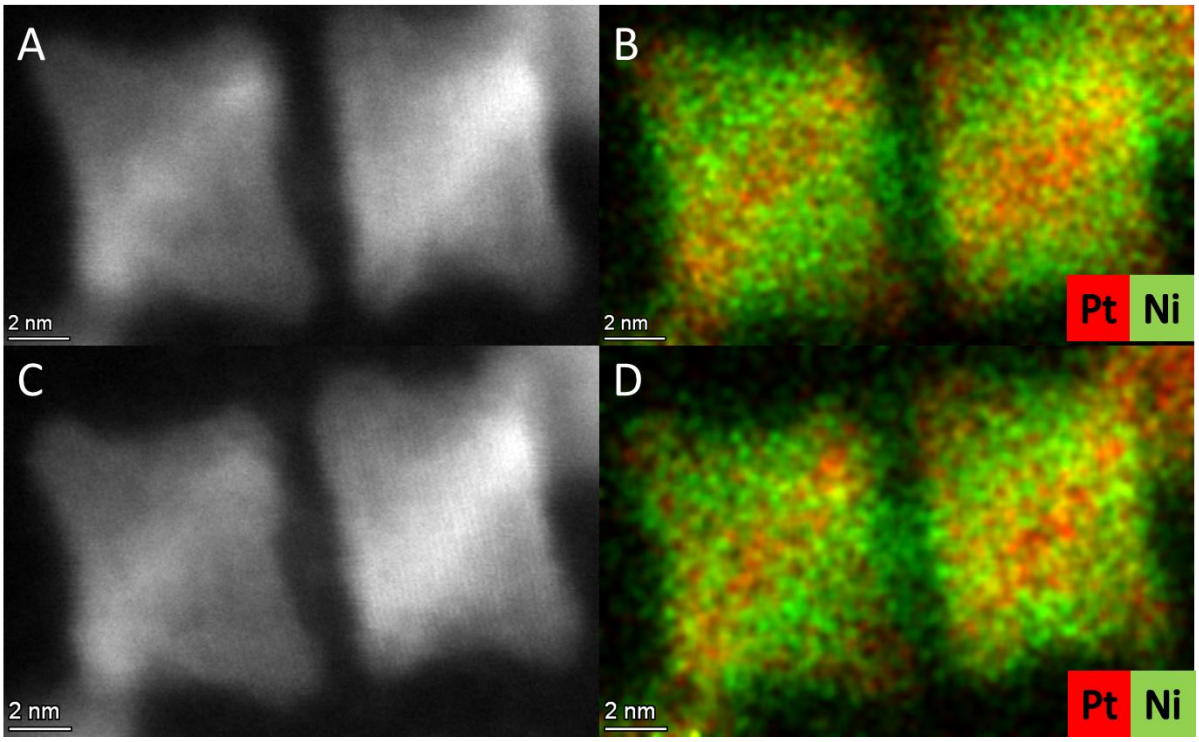

Figure S12 Representative HAADF images and EDX elemental maps of PtNiMoRh-F particles A,B) before and C,D) after 10800 cycles between 0.6 and 0.95 V_{RHE} in Ar-saturated 0.1M $HClO_4$ at identical location. The images were recorded with the Titan G2 80 -200 at an acceleration voltage of 80 kV.

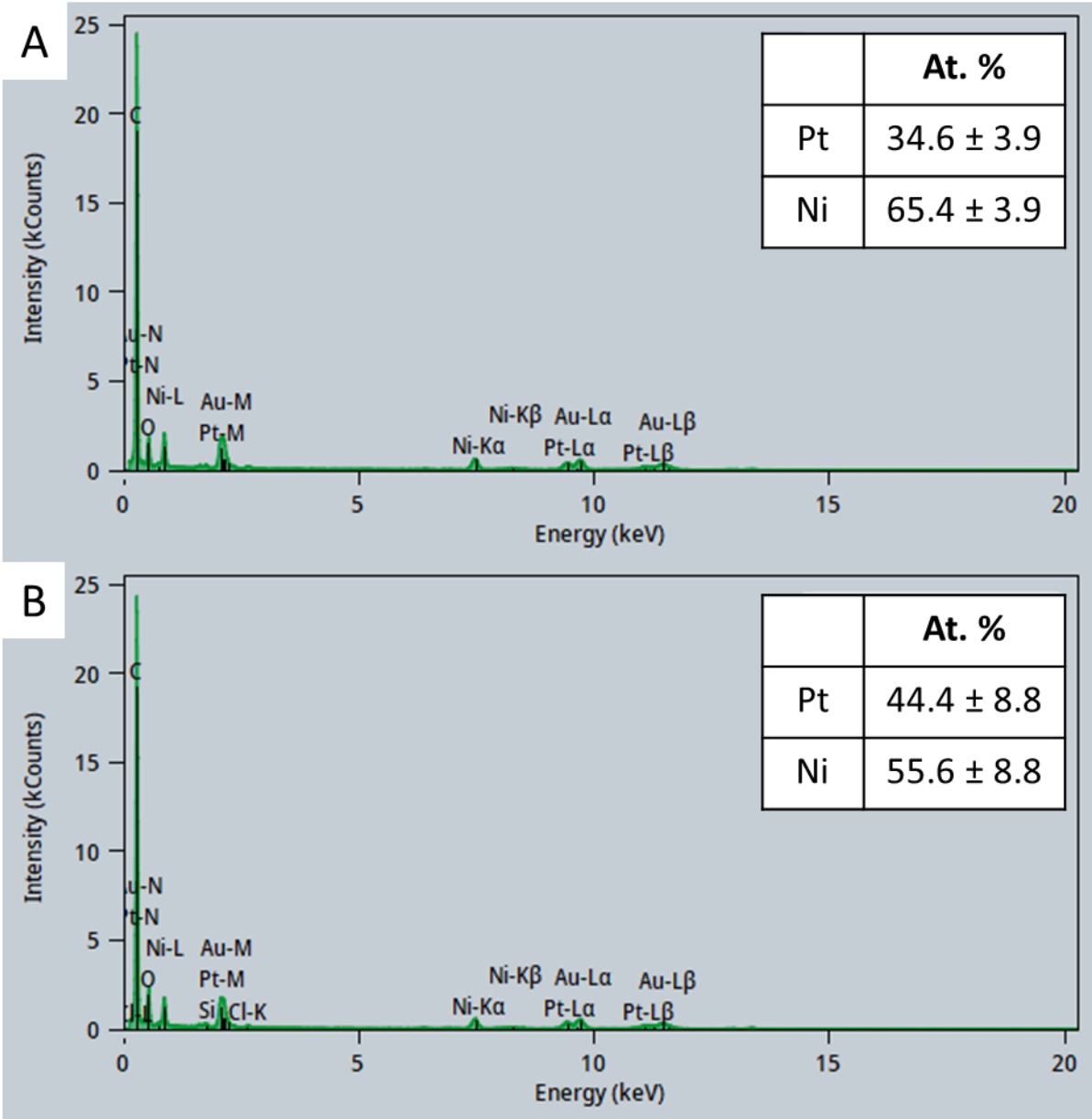

Figure S13 Representative EDX spectra of PtNiMoRh-F before (A) and after (B) an accelerated stress test (AST) consisting of 10800 potential cycles between 0.60 and 0.95 V_{RHE} in Ar-saturated 0.1 M $HClO_4$ at room temperature. Spectra were acquired on a FEI Titan G2 80–200 operated at 80 kV. For quantitative analysis of the Pt/Ni atomic ratio, 10 individual particles were examined before and after the AST at identical locations. The Au and Si peaks originate from the TEM support grid.

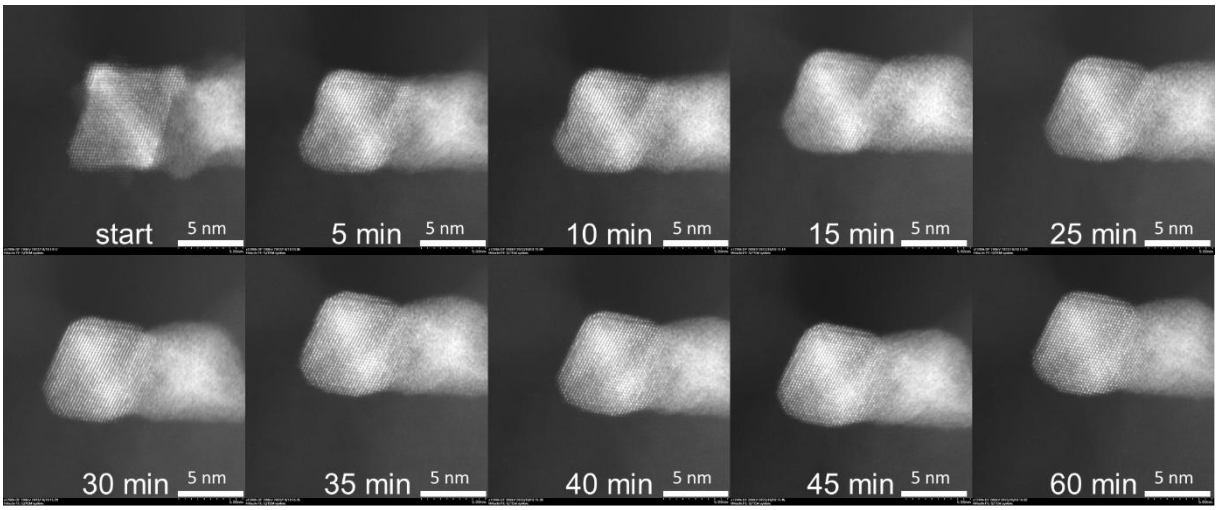

Figure S14 in situ snapshots of the structural evolution of doped PtNiMoRh-F octahedra during heat treatment in a hydrogen atmosphere. The images were taken in an environmental STEM (Hitachi HF5000, 200 kV) at a temperature of 300°C and a hydrogen pressure of approx. 5 Pa.

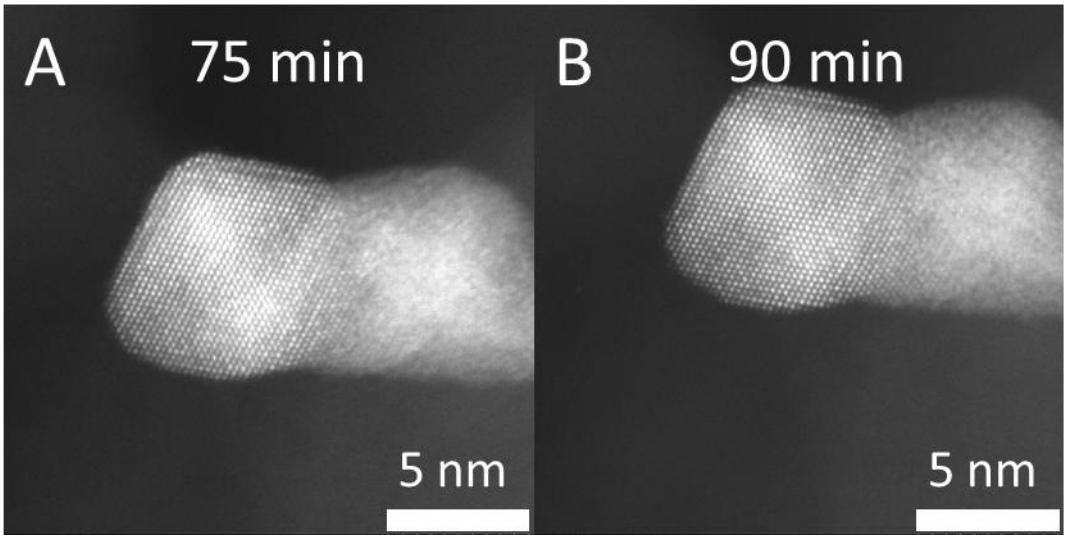

Figure S15 PtNiMoRh particle after 60 min at 300 °C and 15 min at 350 °C in situ heating in hydrogen (left) and after 60 min at 300 °C and 30 min at 350 °C in situ heating in hydrogen (right), performed in a Hitachi HF5000 environmental STEM operated at 80 kV under 5 Pa H_2 atmosphere.

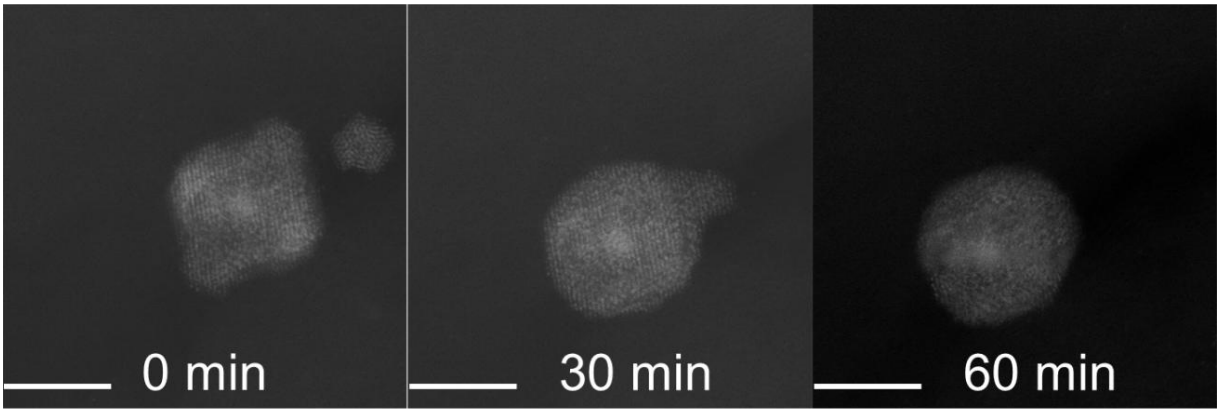

Figure S16 in situ snapshots of the structural evolution of undoped PtNi octahedra during heat treatment in a hydrogen atmosphere. The images were taken in an environmental STEM (Hitachi HF5000, 200 kV) at a temperature of 300°C and a hydrogen pressure of approx. 5 Pa. The scale bar corresponds to 5 nm.

Table 1 Summary of electrochemical data of the pristine catalysts before the heat treatment

Catalyst	Based on H_{upd}				Based on CO stripping				Mass activity / (A/mg_{Pt})	
	ECSA / (m^2/g_{Pt})		Specific activity/ (mA/cm^2)		ECSA / (m^2/g_{Pt})		Specific activity/ (mA/cm^2)			
	Before AST	After AST	Before AST	After AST	Before AST	After AST	Before AST	After AST	Before AST	After AST
PtNi/C-F	33.5	37.1	0.5	0.61	65.9	55.0	0.48	0.73	0.32	0.4
PtNiMoRh/C-F	52.6 ± 10.1	60.8 ± 4.0	2.93 ± 0.1	3.38 ± 0.1	54.8 ± 6.7	56.4 ± 2.5	2.55 ± 0.06	3.75 ± 0.13	1.53± 0.25	2.11 ± 0.14

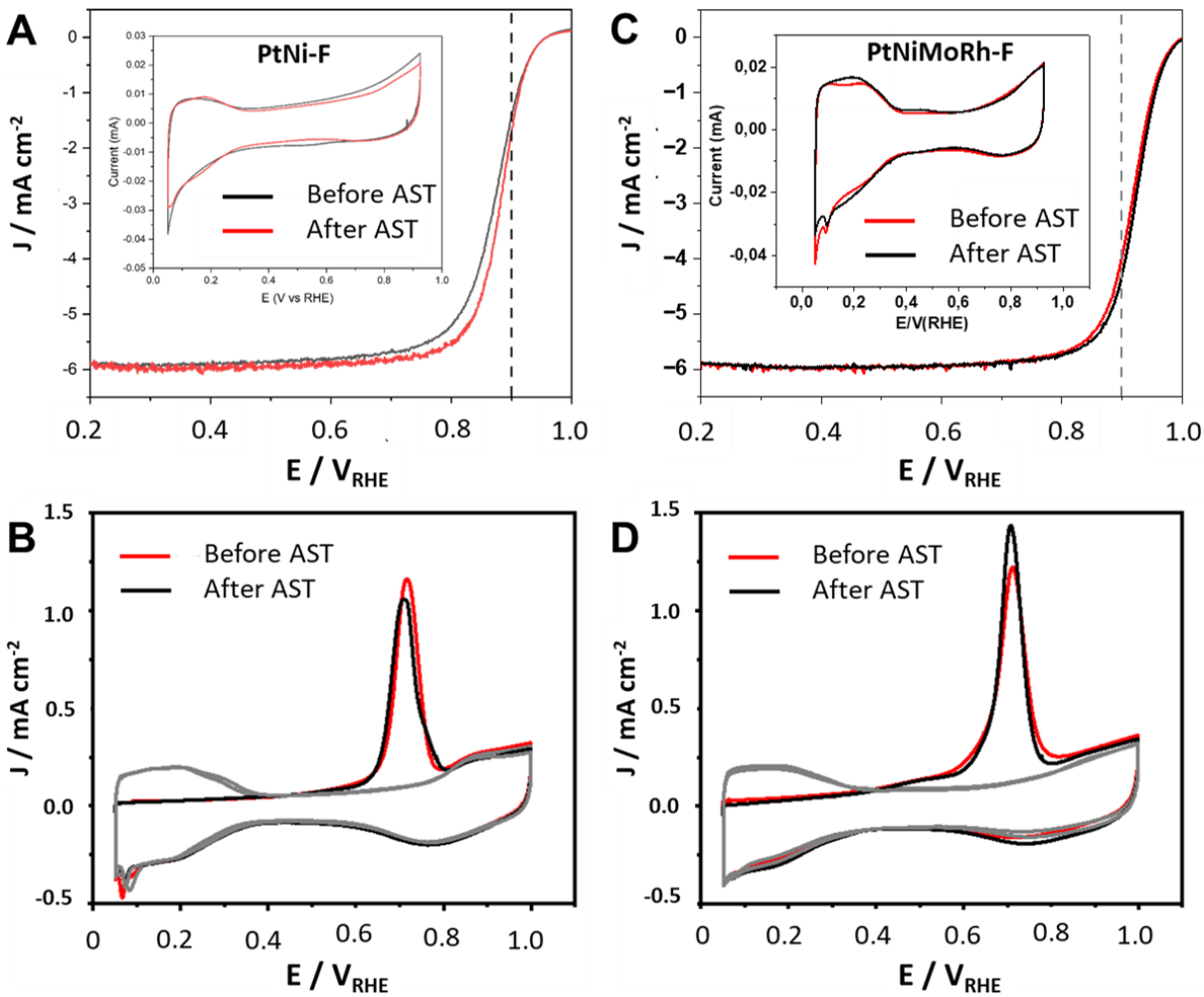

Figure S17 Linear sweep voltammetry curves and CV before and after the stability test of A) PtNi-F and C) PtNiMoRh-F. CO-Stripping curves before and after ASTs for (b) PtNi-F and (d) PtNiMoRh-F catalysts. Adapted from Ref. 1 with permission from the Royal Society of Chemistry

Table S2 Summary of electrochemical data of heat-treated catalysts

Catalyst	Based on H_{upd}				Based on CO stripping				Mass activity / (A/mg_{Pt})	
	ECSA / (m^2/g_{Pt})		Specific activity/ (mA/cm^2)		ECSA / (m^2/g_{Pt})		Specific activity/ (mA/cm^2)			
	Before AST	After AST	Before AST	After AST	Before AST	After AST	Before AST	After AST	Before AST	After AST
PtNi/C-H	41.2± 1.4	43.8± 2.6	5.9± 1.6	3.58± 0.6	37.8± 1.1	37.1± 4.6	6.81± 0.06	4.01± 0.08	2.45± 0.42	1.4± 0.21
PtNiMoRh/C-H	47.9± 0.14	53.8± 0.6	5,9± 1.4	7,03± 1.5	79.8± 0.8	81.6± 6.0	3.72± 0.22	5.23± 0.83	3.06± 0.1	4.24± 0.41

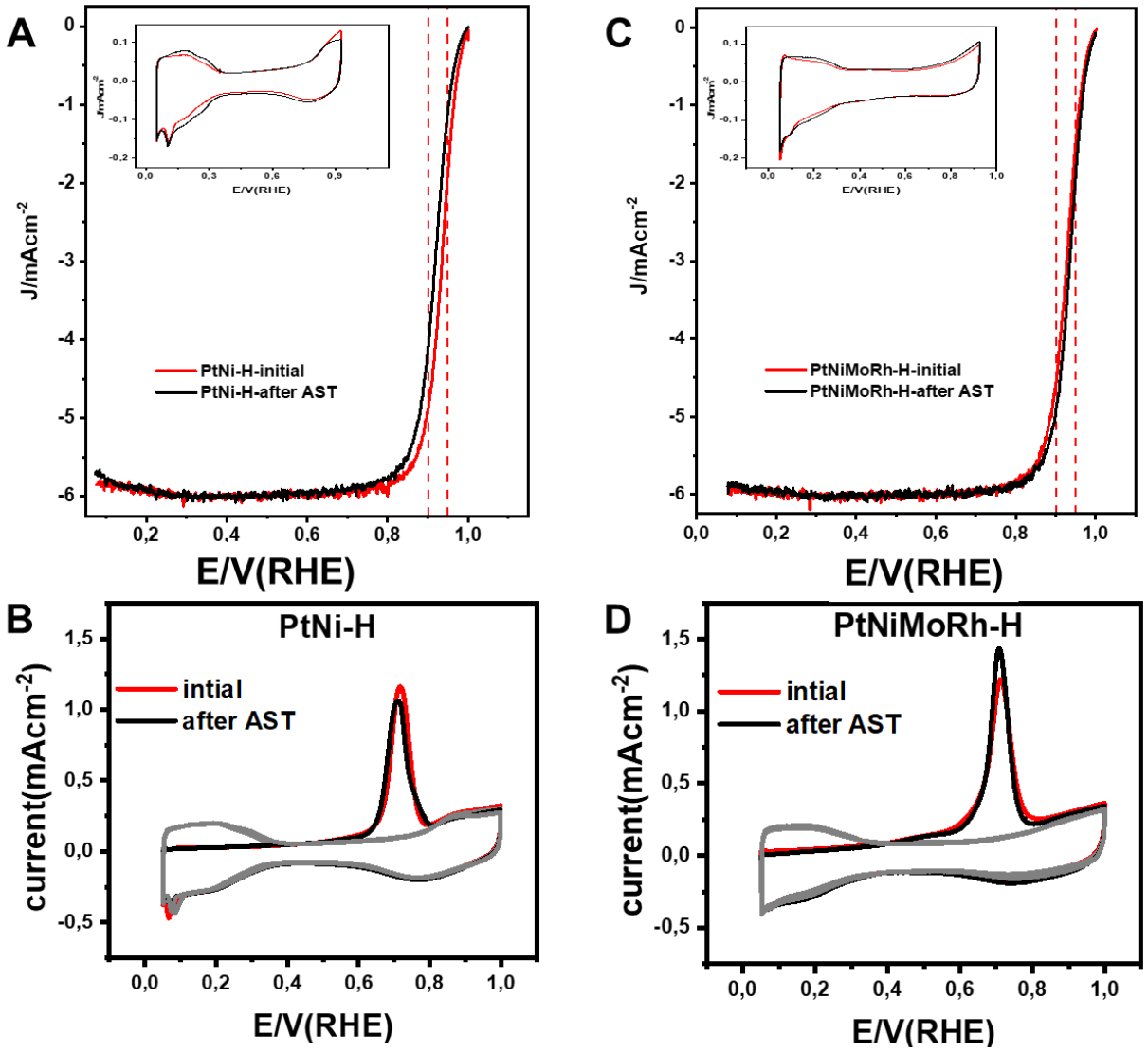

Figure S18 Linear sweep voltammetry curves and CV before and after the stability test of A) PtNi-H and C) PtNiMoRh-H. CO-Stripping curves before and after ASTs for (B) PtNi-H and (D) PtNiRhMo-H catalysts

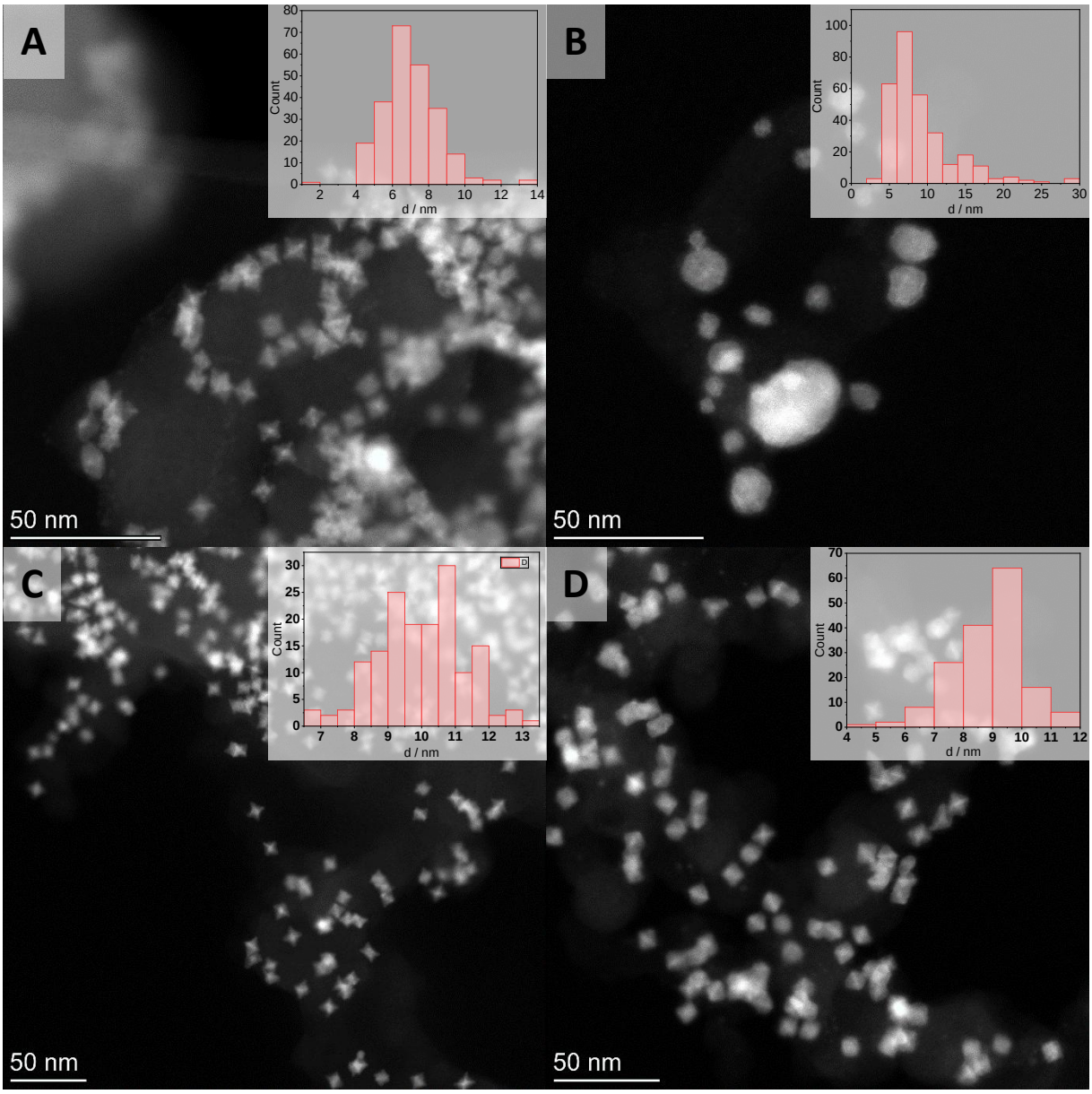

Figure S19 HAADF STEM images and histograms of a) PtNi-F (particle:242, average edge length 6.97 nm ±1.61 nm), b) PtNi-H (particles: 304, average diameter 9.08 nm ± 4.34 nm), c) PtNiMoRh-F(particles: 158, average diameter: 9.97 ± 2.27 nm) and d) PtNiMoRh-H (particles: 168, average diameter: 8.92 ± 1.52 nm).

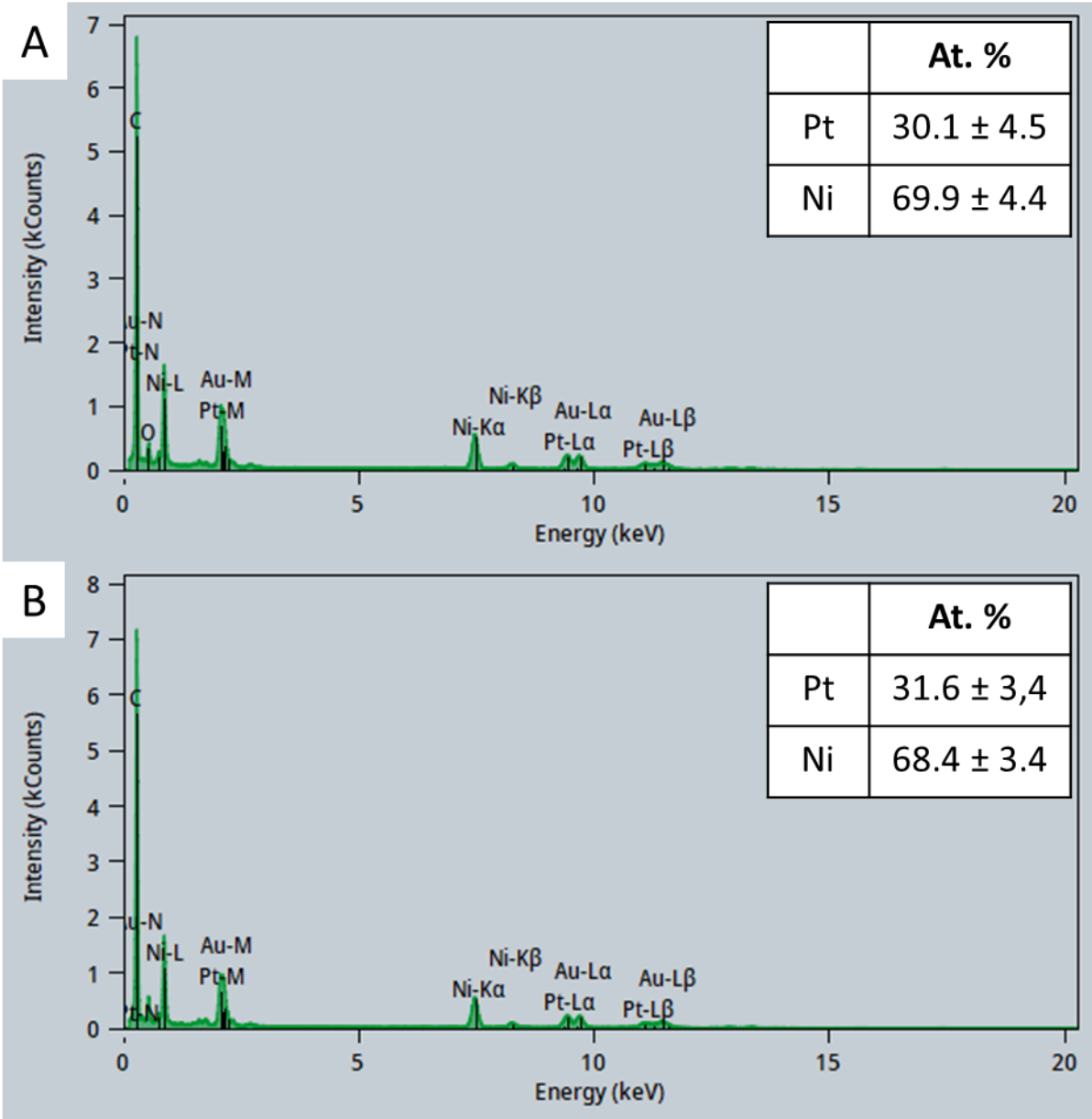

Figure S20 Representative EDX spectra of PtNiMoRh-H before (A) and after (B) an accelerated stress test (AST) consisting of 10800 potential cycles between 0.60 and 0.95 V_{RHE} in Ar-saturated 0.1 M $HClO_4$ at room temperature. Spectra were acquired on a FEI Titan G2 80–200 operated at 80 kV. For quantitative analysis of the Pt/Ni atomic ratio, 10 individual particles were examined before and after the AST at identical locations. The Au and Si peaks originate from the TEM support grid.

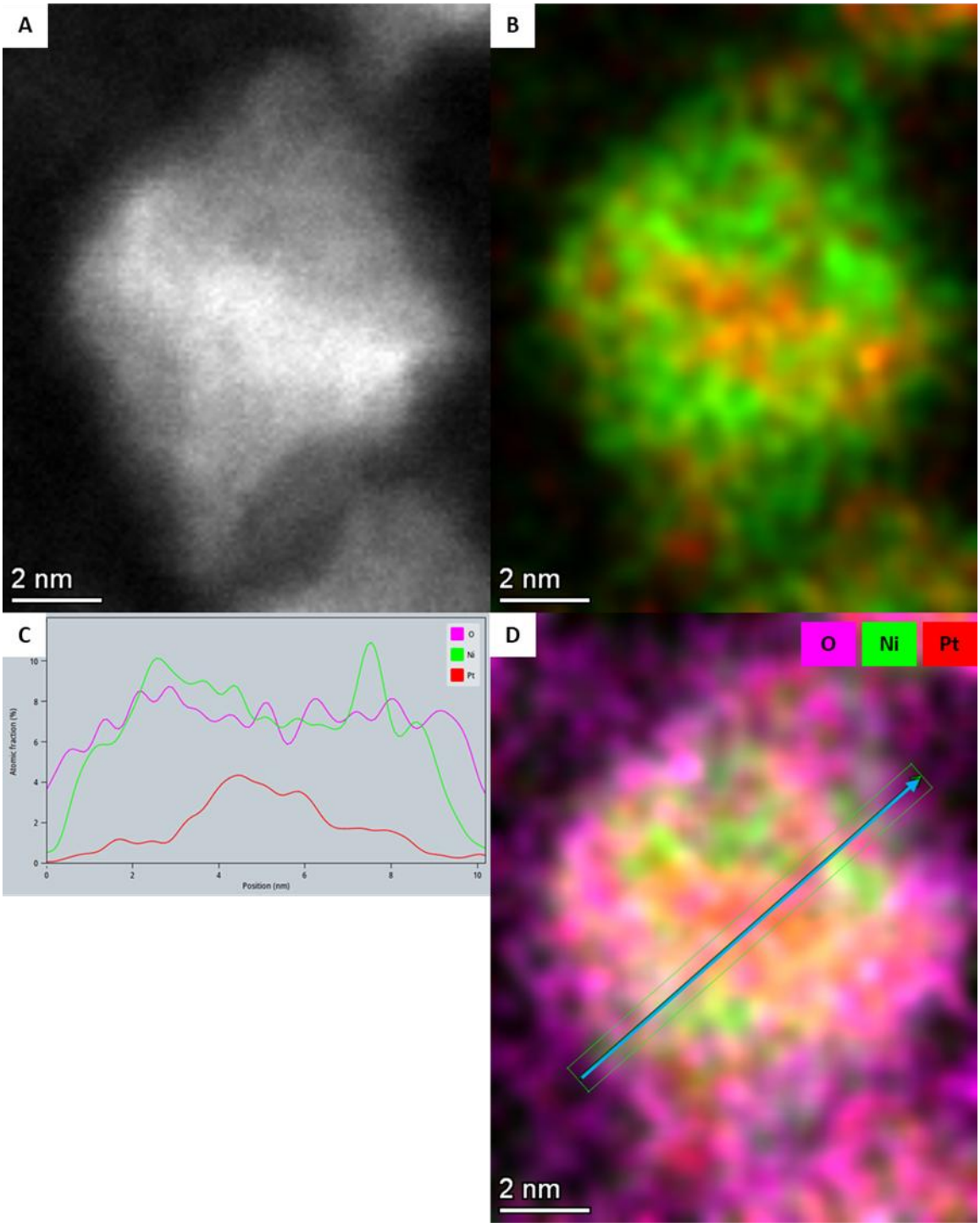

Figure S21 Representative A) HAADF image, B, D) EDX-maps and C) line scan of PtNi-F. The images were recorded with the Titan G2 80 -200 at an acceleration voltage of 80 kV.

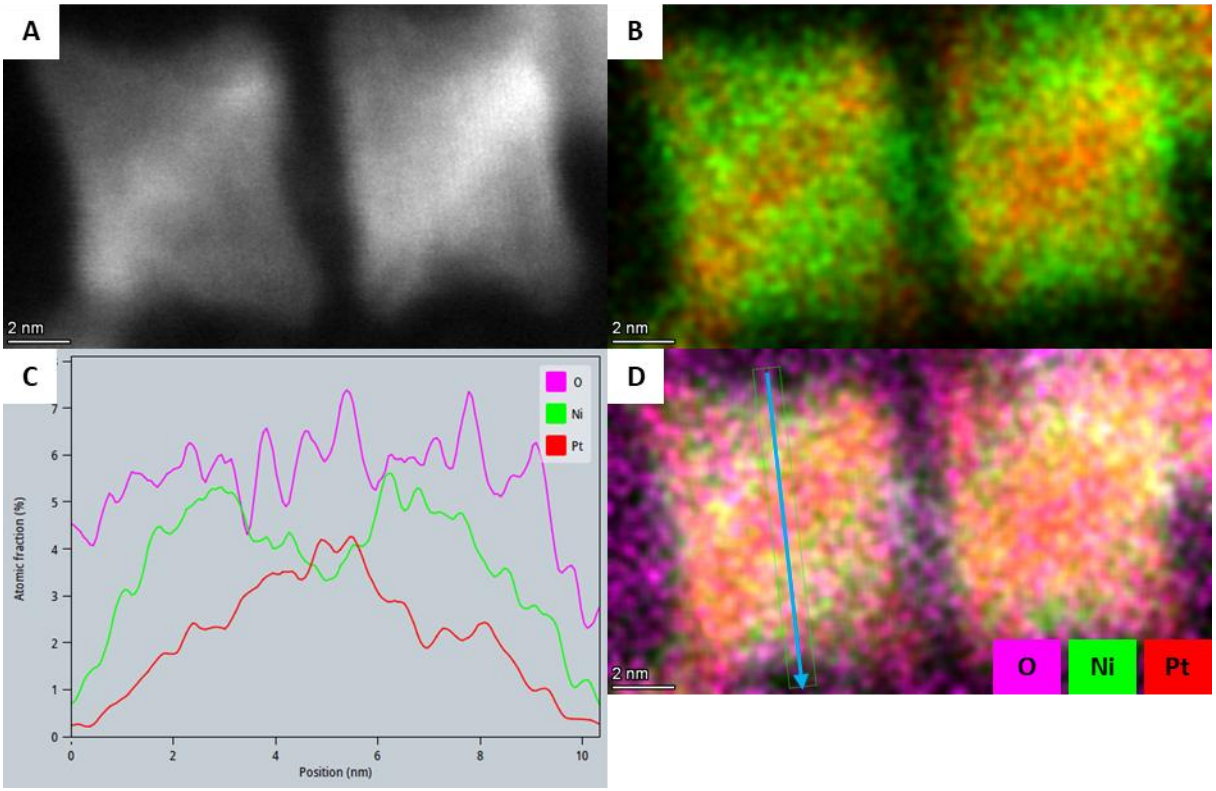

Figure S22 Representative A) HAADF image, B, D) EDX-maps and C) line scan of PtNiMoRh-F. The images were recorded with the Titan G2 80 -200 at an acceleration voltage of 80 kV.

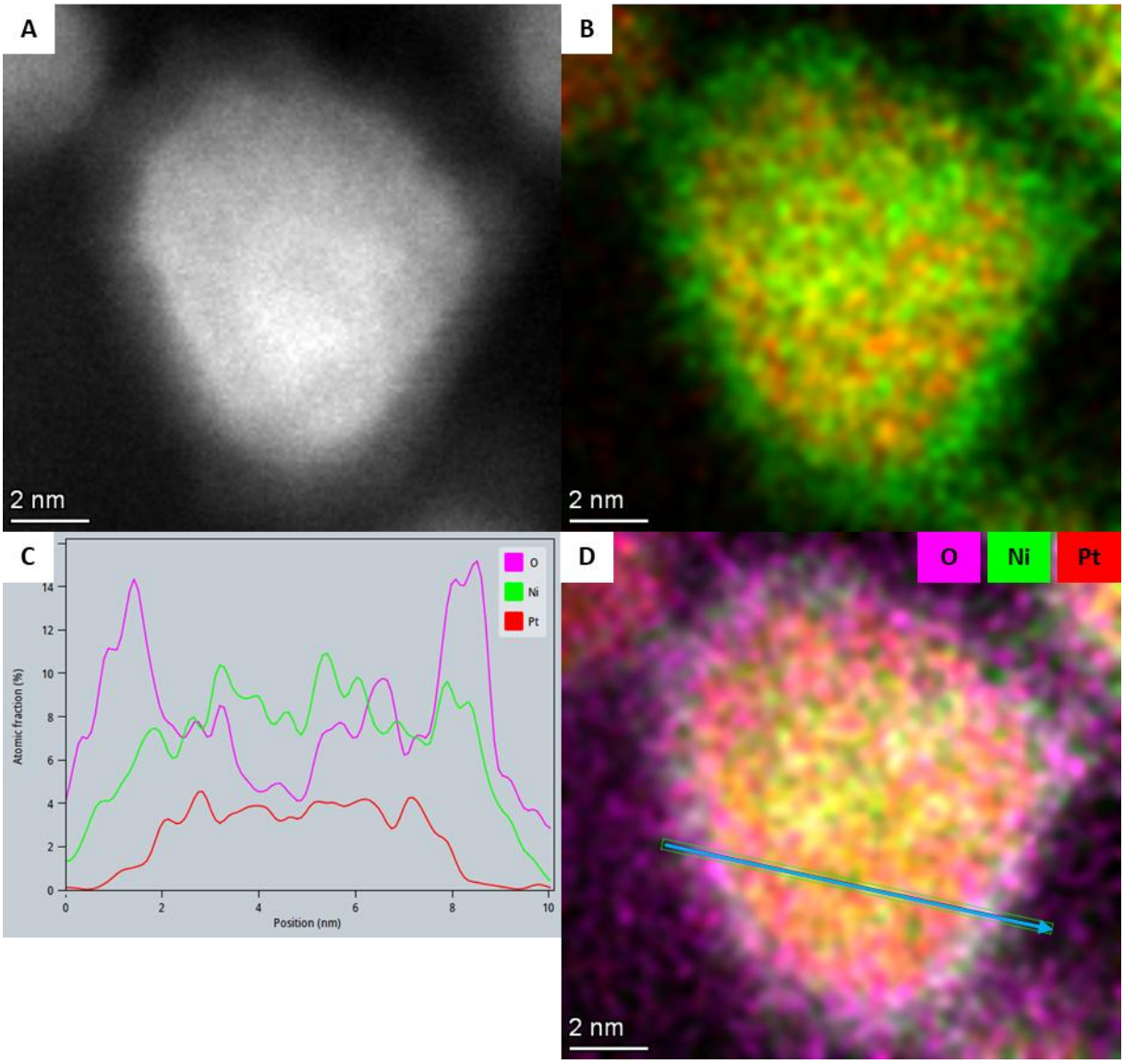

Figure 23 Representative A) HAADF image, B, D) EDX-maps and C) line scan of PtNi-H. The images were recorded with the Titan G2 80 -200 at an acceleration voltage of 80 kV.

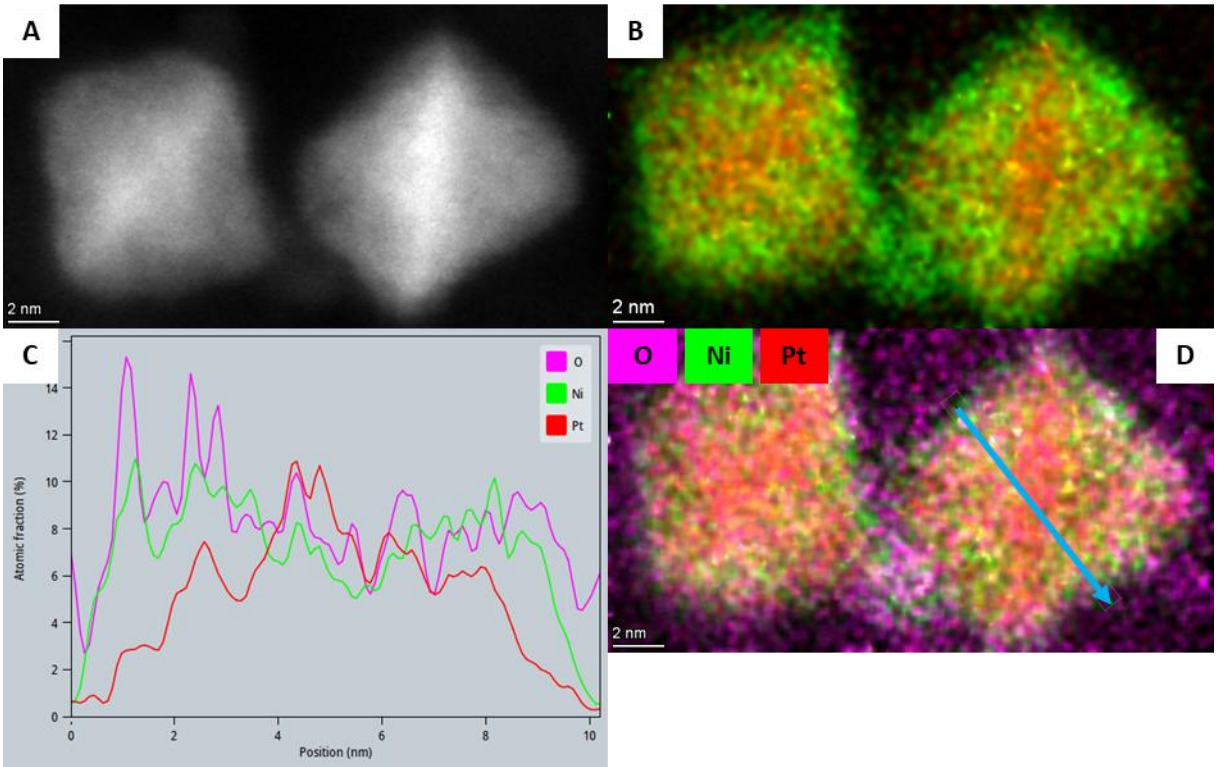

Figure 24 Representative A) HAADF image, B, D) EDX-maps and C) line scan of PtNiMoRh-H. The images were recorded with the Titan G2 80 -200 at an acceleration voltage of 80 kV.

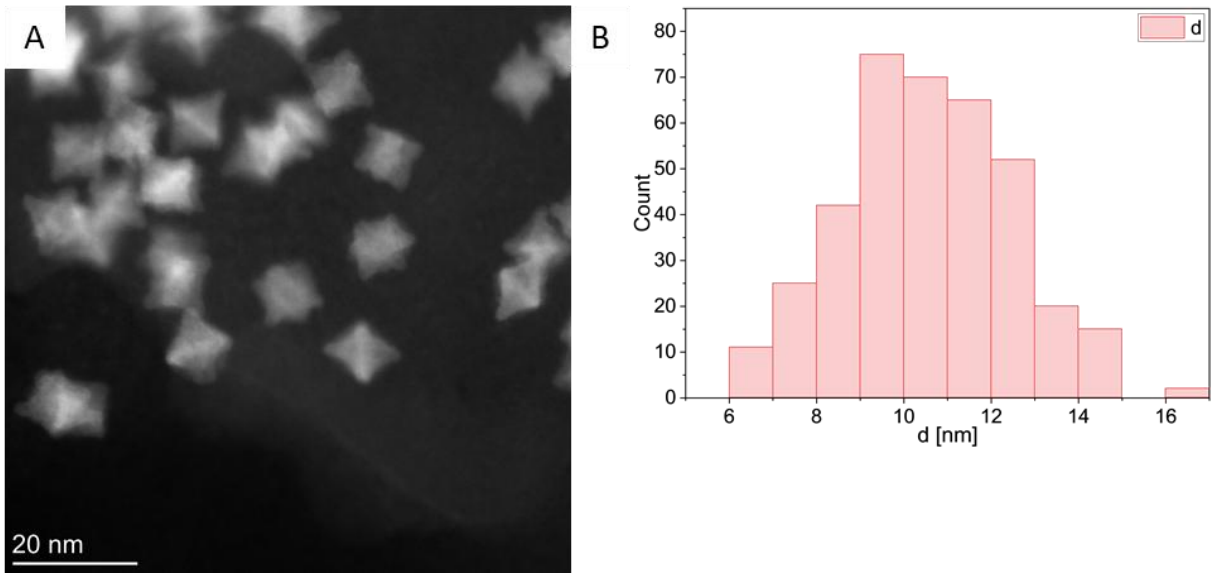

*Figure S25 Representative A) HAADF image and B) particle size distribution of PtNiMoRh-F after the identical location STEM AST (10800 cycles between 0.6 and 0.95 V_{RHE} in Ar-saturated 0.1M $HClO_4$). The images were recorded with the Titan G2 80 -200 at an acceleration voltage of 80 kV. The average particle diameter is **10.4 nm ± 2.0** nm and 377 particles were evaluated.*

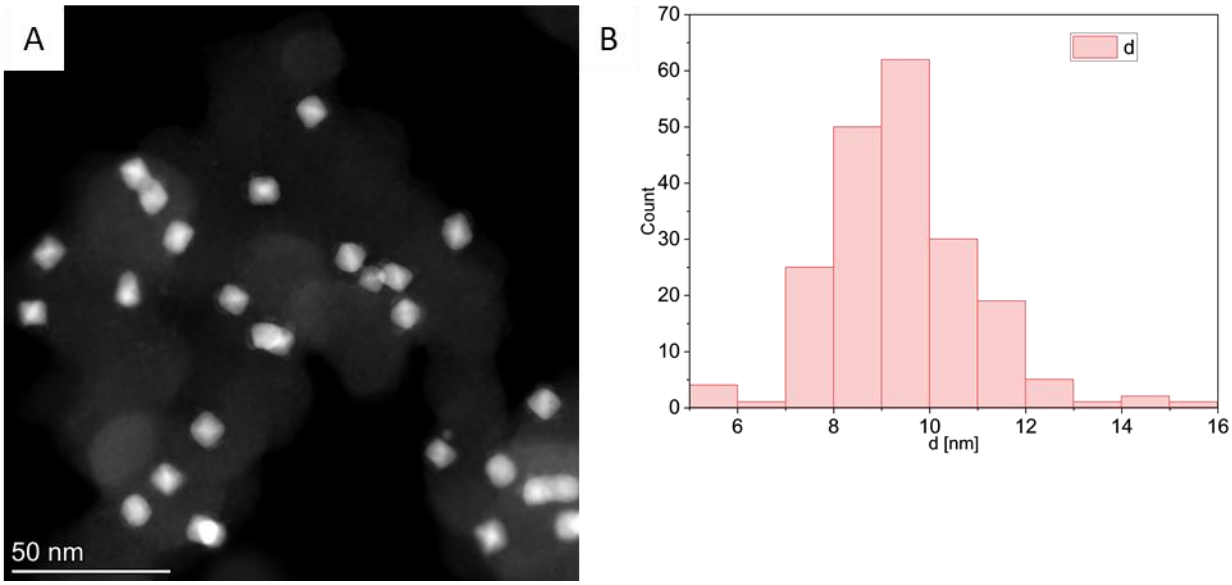

*Figure S26 Representative A) HAADF image and B) particle size distribution of PtNiMoRh-H after the identical location STEM AST (10800 cycles between 0.6 and 0.95 V_{RHE} in Ar-saturated 0.1M $HClO_4$). The images were recorded with the Titan G2 80 - 200 at an acceleration voltage of 80 kV. The average particle diameter is **9.4 nm ± 1.4** nm and 201 particles were evaluated.*

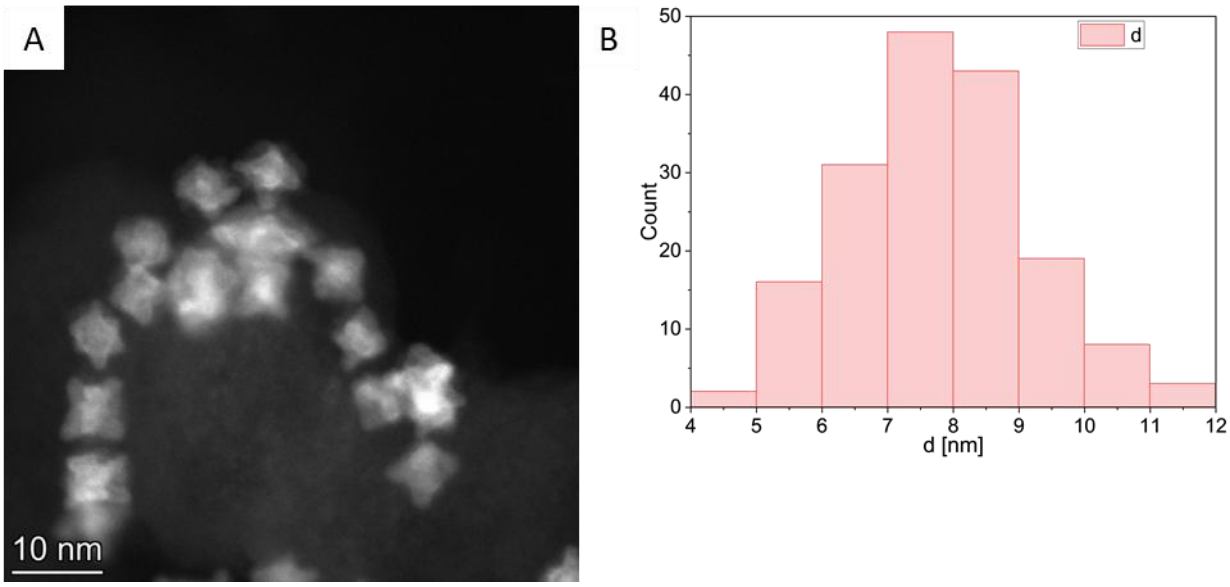

*Figure S27 Representative A) HAADF image and B) particle size distribution of PtNi-F after the identical location STEM AST (10800 cycles between 0.6 and 0.95 V_{RHE} in Ar-saturated 0.1M $HClO_4$). The images were recorded with the Titan G2 80 -200 at an acceleration voltage of 80 kV. The average particle diameter is **7.7 nm ± 1.5** nm and 170 particles were evaluated.*

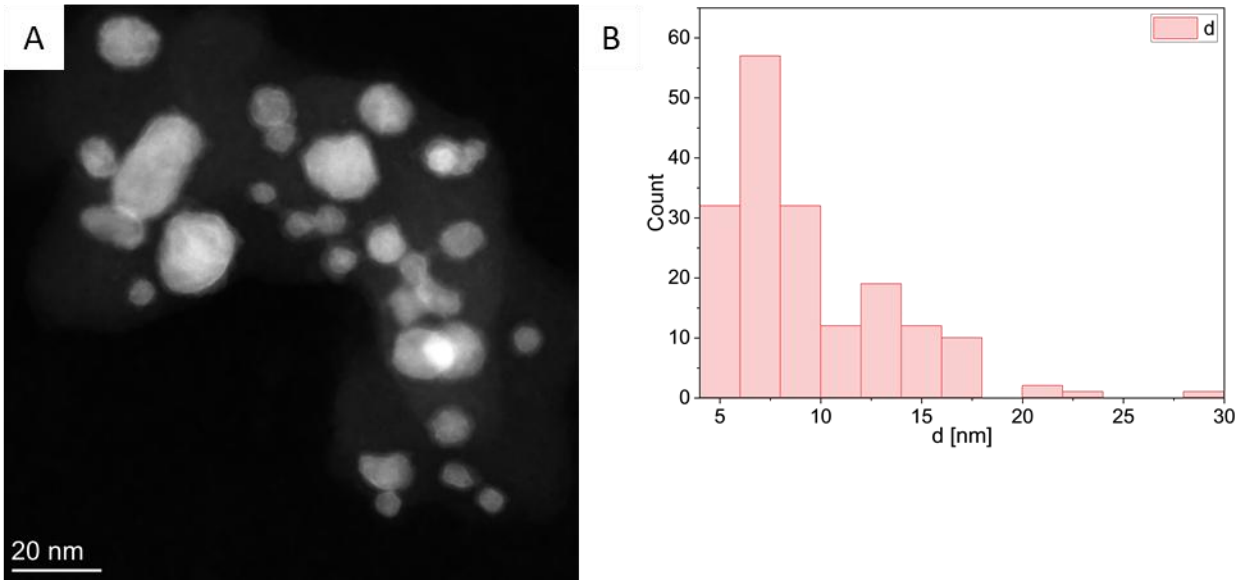

*Figure 28 Representative A) HAADF image and B) particle size distribution of PtNi-H after the identical location STEM AST (10800 cycles between 0.6 and 0.95 V_{RHE} in Ar-saturated 0.1M $HClO_4$). The images were recorded with the Titan G2 80 -200 at an acceleration voltage of 80 kV. The average particle diameter is **9.4 nm ± 4.1 nm** and 178 particles were evaluated.*

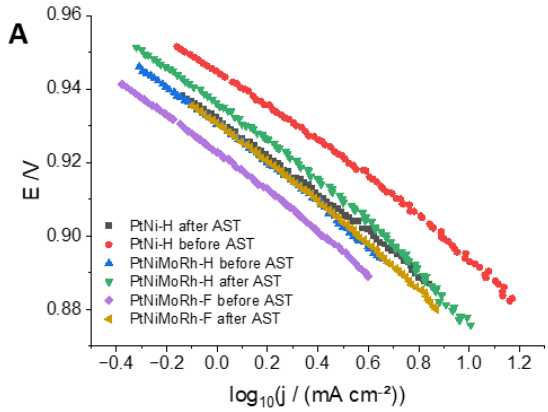

B

	$b_{initial}$ / mV dec^{-1}	b_{after} / mV dec^{-1}
PtNi-H	50.6 ± 5.0	50.8 ± 1.1
PtNiMoRh-F	51.1 ± 1.1	53.9 ± 2.2
PtNiMoRh-H	51.3 ± 2.1	51.8 ± 3.8

Figure S29 A) Tafel plots derived from ORR polarization curves of the catalyst before and after STs. Tafel slope b was obtained from linear fits of E vs. log_{10} (j/ (mA cm^{-2})) in the kinetic-controlled regime. For PtNi-F, no Tafel analysis was performed due to data availability. B) Summary of calculated Tafel slopes.

References

1. Hornberger, E. *et al., Chem. Sci., 2022,**13**, 9295-9304.*
2. Macarthur, K. *et al. ACS Appl. Energy Mater. 2023,* **6***, 11, 5959–5967.*
3. POLANI, S. et al. *ACS Catalysis*, 2021, **11,** 11407-11415.
4. RUDI, S, et al., Electrocatalysis, 2014, 5, 408-418.